Jamming transition in emulsions and granular materials

H. P. Zhang

Physics Department, City College of New York, New York 10031, USA

H. A. Makse

Physics Department and Levich Institute, City College of New York, New York 10031, USA

(Received 16 January 2005; published 7 July 2005)

We investigate the jamming transition in packings of emulsions and granular materials via molecular dynamics simulations. The emulsion model is composed of frictionless droplets interacting via nonlinear normal forces obtained using experimental data acquired by confocal microscopy of compressed emulsions systems. Granular materials are modeled by Hertz-Mindlin deformable spherical grains with Coulomb friction. In both cases, we find power-law scaling for the vanishing of pressure and excess number of contacts as the system approaches the jamming transition from high volume fractions. We find that the construction history parametrized by the compression rate during the preparation protocol has a strong effect on the micromechanical properties of granular materials but not on emulsions. This leads the granular system to jam at different volume fractions depending on the histories. Isostaticity is found in the packings close to the jamming transition in emulsions and in granular materials at slow compression rates and infinite friction. Heterogeneity of interparticle forces increases as the packings approach the jamming transition which is demonstrated by the exponential tail in force distributions and the small values of the participation number measuring spatial localization of the forces. However, no signatures of the jamming transition are observed in structural properties, like the radial distribution functions and the distributions of contacts.

I. INTRODUCTION

A variety of systems such as granular materials, compressed emulsions, or molecular glasses, exhibit a nonequilibrium transition from a fluidlike to a solidlike state. When the constituent particles of such systems are so crowded that they are in close contact with one another, the whole system experiences a sudden dynamical arrest, which is referred to as the glass or jamming transition [1–3]. A jammed system is a many-body system blocked in a configuration far from equilibrium, from which it takes too long a time to relax in the laboratory time scale. Jammed systems are usually random packings of particles, which have been the starting point for many studies of liquids and glasses [3–7]. A theoretical approach to treat these systems has been developed by Edwards and co-workers [8,9] who have proposed a statistical mechanics description of such jammed system, in which thermodynamic quantities are computed as flat average over jammed configurations [10–12].

In a recent paper [13] we found that the jamming transition in packings of granular materials and emulsions can be viewed as a phase transition at the critical concentration of random close packing for frictionless emulsions or random loose packing for frictional grains. The transition is characterized by a power-law behavior and the corresponding set of exponents describing the stress, coordination number, and elastic moduli as the system approaches the jamming transition. This idea has also been investigated for packings of frictionless particles [14,15] and colloids [16]. Here we elaborate further on the results of [13] and present our detailed computer simulation studies about many aspects of the jamming transitions in these systems.

We consider packings of spherical deformable particles interacting via friction and frictionless forces. Granular packings are characterized by elastic Hertz-Mindlin forces [17–19] with Coulomb friction. Concentrated emulsion systems are modeled as a collection of frictionless deformable droplets interacting via a nonlinear normal force law which is obtained from the analysis of experimental data acquired using confocal microscopy in [20].

We first introduce a protocol to generate a series of packings near the jamming transition and beyond for both emulsions and granular materials. Then we study how the construction history of the packings affects the jamming transition. The existence of frictional tangential forces is one of many generic properties of granular materials. In the elastic Hertz-Mindlin model the tangential force is proportional to the tangential displacement, and it is truncated by a Coulomb cutoff. Both the elastic tangential force and Coulomb friction are path dependent. The path dependence in the microscopic interactions leads to the path dependence of the granular packings at the macroscopic level, an effect that has been shown in several classical experiments [5,6,21]. In our simulations we find that the construction history affects the properties at the jamming transition in the granular packings through their direct impact on the tangential forces, while in the case of emulsions we do not find any path dependence.

Next, we fully characterize the evolution of the micromechanical and microstructural properties, such as the stress, the coordination number and isostaticity, the radial distribution function, the probability distributions of normal and tangential forces and interparticle contacts, the existence of force chains, the participation number and plasticity index, as the system approaches the jamming transition. We found that the heterogeneity of interparticle forces increases as the packings approach the jamming transition which is demonstrated by the exponential tail in force distributions and the

small values of the participation number. However, no clear signatures of the jamming transition are observed in structural properties, like the radial distribution functions and the distributions of contacts.

The paper is organized as follows. In Sec. II we discuss the microscopic force models used in our simulations of granular materials and emulsions. In Sec. III we give the details of the numerical protocol to generate packings near the jamming transition and beyond and the various measurements to be performed. The main results of this work are given in Sec. IV and we summarize our results in Sec. V.

II. MICROSCOPIC MODEL

In this section we discuss the microscopic models of interparticle forces for granular materials and emulsions. We first briefly review the standard Hertz-Mindlin model for granular materials; more details can be found in [17,19,22]. Then we describe the linear "Princen model" [23] for the interparticle forces in emulsions and its nonlinear modification according to experimental data on deformation in concentrated emulsion systems [20].

A. Contact mechanics in granular materials

We describe the microscopic interaction between grains by the nonlinear Hertz-Mindlin normal and tangential forces. The normal force between two contacting grains at position $\vec{x}_1$ and $\vec{x}_2$ with uncompressed radii R_1 and R_2 is [17,22]

$$F_n = \frac{2}{3} k_n R^{1/2} \xi^{3/2}, \qquad (1)$$

where R is the geometric mean of R_1 and R_2, $R = 2R_1 R_2/(R_1+R_2)$, and ξ is the normal overlap, $\xi = (1/2)[R_1 + R_2 - |\vec{x}_1 - \vec{x}_2|]$. The normal force acts only in compression, i.e., $F_n = 0$ when $\xi < 0$. The effective stiffness $k_n = 4G/(1-\nu)$ is defined in terms of the shear modulus of the grains G and the Poisson ratio ν of the material from which the grains are made. From Eq. (1), we can see that the normal forces are completely determined by the geometrical configuration of the packing and have nothing to do with the construction history.

The tangential contact force was first calculated by Mindlin [18] for grains under oblique loading. In his model, the increment in tangential force is

$$\Delta F_t = k_t (R\xi)^{1/2} \Delta s \qquad (2)$$

where $k_t = 8G/(2-\nu)$, and the variable s is defined such that the relative tangential displacement between the two grain centers is $2s$. Therefore the tangential force is obtained by integrating Eq. (2) over the path taken by the particles in contact with the initial condition, $F_n = 0$, $F_t = 0$ at $\xi = 0$, $s = 0$, yielding

$$F_t = \int_{path} k_t (R\xi)^{1/2} ds. \qquad (3)$$

As the tangential displacement increases, the elastic tangential force F_t reaches its limiting value given by a Coulomb cutoff for granular materials, which is

$$F_t = \mu F_n. \qquad (4)$$

The Coulomb cutoff adds a second source of path dependence to the problem.

From the discussion above, one can see that a straightforward way to affect the tangential force is to change the frictional coefficient μ, which controls the maximum value of the ratio between tangential and normal force. But the elastic tangential force Eq. (2) is even more intimately related to the tangential displacement, which is mainly determined by the construction history.

B. Force law for emulsion

Emulsions are a class of material that is both industrially important and exhibits very interesting physics [23]. They belong to the wider material class of colloids in that they consist of two immiscible phases one of which is dispersed into the other, the continuous phase. Both of the phases are liquids and their interface is stabilized by the presence of surface-active species. Emulsions are composed of droplets of a liquid (for instance silicone oil) stabilized by a surfactant (like sodium dodecylsulfate) in a continuum phase (such as a water and glycerol mixture) [20]. Being composed of only liquids, emulsion droplets interact with each other only via normal forces with no solid friction between them. The determination of an accurate force model for the compression of two droplets is by no means trivial, but it can be simplified in certain limits. For small deformation with respect to the droplets surface area the Laplace pressure remains unchanged and all energy of the applied stress is presumed to be restored in the deformation of the surface. Then the normal repulsive force between two spherical droplets in contacts with uncompressed radii R_1 and R_2 can be calculated at the microscopic level as

$$f = \frac{\sigma}{R} A_{mea}. \qquad (5)$$

This is known as the Princen model [23], where σ is the interfacial tension of droplets, f is the normal force between two droplets, R is the geometric mean of R_1 and R_2, and A_{mea} is the measured contact area between the droplets. As in the granular materials, the normal force acts only in compression.

In [20] a linear model was used to relate the area of deformation with the overlap between the spheres ξ, resulting in a linear spring model for the force law between the droplets. More detailed calculations [24] and numerical simulations [25] show that the interdroplet forces in emulsions are better represented by a nonlinear spring $f \propto \xi^\alpha$ with the exponent α between 1 and 1.5 and, more importantly, depending on the number of contact forces acting on the droplet.

Recently, Brujić *et al.* [20] used confocal microscopy to study a compressed polydisperse emulsion. This system consists of a dense packing of emulsion oil droplets, with a sufficiently elastic surfactant stabilizing layer to mimic solid particle behavior, suspended in a continuous phase fluid. By refractive index matching of the two phases they obtained a three-dimensional (3D) image of the packing structure by
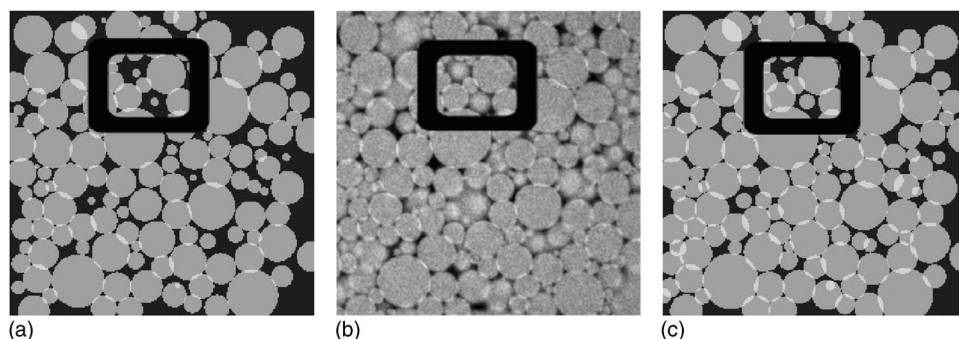
FIG. 1. Image slice of emulsion packing from confocal microscope (b); reconstructed image before (a) and after Monte Carlo annealing (c).

using confocal microscopy for the imaging of the droplet packings at varying external pressures, i.e., volume fractions. The key feature of this optical microscopy technique is that only light from the focal plane is detected. Thus 3D images of translucent samples can be acquired by moving the sample through the focal plane of the objective and acquiring a sequence of 2D images. One 2D image obtained experimentally is shown in Fig. 1(b).

The emulsion system, stable to coalescence and Ostwald ripening, consisted of silicone oil droplets [$\eta = 10$ centistoke (cS)] in a refractive index matching solution of water ($w_t = 51\%$) and glycerol ($w_t = 49\%$), stabilized by 20 mM sodium dodecylsulfate upon emulsification and later diluted to below the critical micellar concentration of 13 mM to ensure a repulsive interdroplet potential. The droplet phase is fluorescently dyed using Nile Red, prior to emulsification. The control of the particle size distribution, prior to imaging, is achieved by applying very high shear rates to the sample, inducing droplet breakup down to a radius mean size of 3.4 μm. This system is a modification of the emulsion reported by Mason *et al.* [26] to produce a transparent sample suitable for confocal microscopy.

In these images, the area of contacts, the droplets and the aqueous background differ by the darkness in an eight-bit gray-scale image such as the one displayed in Fig. 1(a) which has an average darkness 210, 90, and 30, respectively. The result of the image analysis carried out by Brujić *et al.* is a set of contact areas A_{mea} along with the undeformed radii (R_1, R_2) and positions ($\vec{x}_1, \vec{x}_2$) of two droplets giving rise to each contact. Using the obtained information of R_i and $\vec{x}_i$ and ignoring the droplet deformations, we can reconstruct the images as shown in Fig. 1(b) and calculate a geometric overlapping area

$$A_{cal} = \pi R \xi, \qquad (6)$$

where ξ is the overlapping. For all the 1439 contacts obtained in the experiments, A_{cal} is plotted against A_{mea} in the inset of Fig. 2, from which we can see that A_{cal} is generally different from A_{mea}, indicating that there exist deviations from the linear force law Eq. (5). This fact provides a direct measure of the effects of anharmonicity of interaction between the droplet surfaces.

In order to extract the nonlinear dependence of the force law between the force and the deformation characterized by ξ, we plot the calculated area A_{cal} from the reconstructed image versus the real area of deformation A_{mea}. In order to

achieve this, we need to improve the estimation of the droplet centers and radii by minimizing the difference between the reconstructed image and the original one. In this minimization, R_i and $\vec{x}_i$ are the changing variables and we use a Monte Carlo annealing method to find the optimum set of parameters. The corresponding image after the minimization is shown in Fig. 1(c), which is closer to the original image than the reconstructed image shown in Fig. 1(a) as indicated by the rectangular region in the figures. Finally, we choose only those contacts for which R_i and $\vec{x}_i$ change less than 5% before and after the minimization, and plot A_{cal} versus A_{mea} in the main panel of Fig. 2. The plot shows a clear trend which can be fitted as

$$A_{cal} = 2.67(A_{mea})^{0.78}. \qquad (7)$$

Combining Eqs. (5), (6), and (7), we obtain the nonlinear force law for emulsion droplets:

$$f = 1.23 \sigma \tilde{R}^{0.28} \xi^{1.28}. \qquad (8)$$

In our simulations, Eq. (8), which takes in account partially the effects of the anharmonicity of interaction between the droplets, is used. We also use a linear spring force law $f = 4\pi\sigma\xi$, which completely neglects the anharmonicity of interaction. These two forces give similar results. In this paper, we only present the results using Eq. (8).
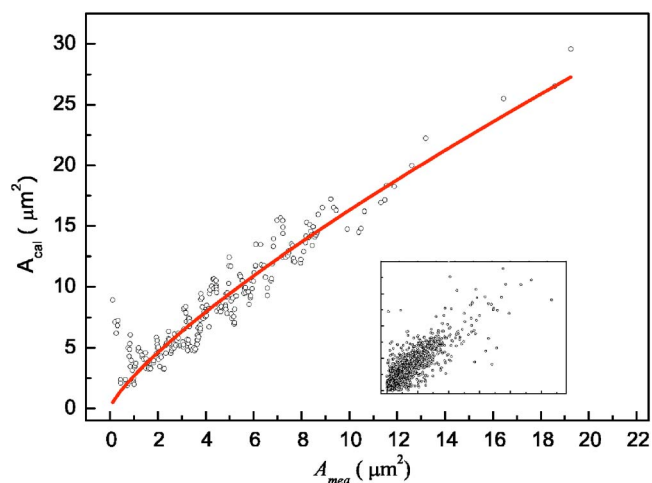

FIG. 2. (Color online) A_{cal} is plotted against A_{mea} after Monte Carlo annealing; the line is a fit of Eq. (7). In the inset, A_{cal} is plotted against A_{mea} for all forces before Monte Carlo annealing.

III. SIMULATIONS, PROTOCOL AND MEASUREMENTS

In this section, we first describe the method of molecular dynamics (MD) simulations. Then we show the protocol to generate packings approaching the jamming transition, and in the third part we define various quantities we use to characterize the jamming transition.

A. Molecular dynamics simulation

We follow the discrete element method (DEM) or molecular dynamics developed by Cundall and Strack [27] and solve the Newton equations for an ensemble of particles with zero gravity, which interact via the microscopic models discussed in Sec. II. The DEM employs a time-stepping, finite-difference approach to solve the Newton equations of motion simultaneously for every particle in the system:

$$\vec{F} = m \frac{d^2 \vec{X}}{dt^2},$$ (9)

$$\vec{M} = I \frac{d^2 \vec{\theta}}{dt^2}$$ (10)

where $\vec{F}$ and $\vec{M}$ are the total force and torque acting on a given particle, m and I are the mass and moment of inertia, and $\vec{X}$ and $\vec{\theta}$ are the position and angle of the particles, respectively. The numerical solutions of Eqs. (9) and (10) are obtained by integration, assuming constant velocities and accelerations for a given time step. We choose the time step to be a fraction of the time that it takes for sound waves to propagate on one grain (or droplet). A global damping proportional to the translational velocity was used to dissipate energy in both cases. The damping simulates the drag force from the suspending medium, i.e., water-glycerol mixture in emulsions and ambient air in granular materials. We constrain the global damping to be small enough not to have any effect on results presented in this paper. More details about the simulations can be found in [19].

In the simulations of emulsions, the system consists of 10 000 droplets, which are all 2 μm in diameter. Droplets interact via the normal force given by Eq. (8) with the interfacial tension $\sigma = 9.8 \times 10^{-3}$ N/m and the density $\rho = 10^3$ kg/m^3. The granular system is composed of 10 000 glass beads of equal size (radius 0.1 mm) interacting via the Hertz-Mindlin forces Eqs. (1) and (3) and the Coulomb force Eq. (4). The microscopic parameters defining the glass beads are the shear modulus $G = 29$ GPa, the Poisson ration $\nu = 0.2$, the friction coefficient $\mu = 0.3$, and the density $\rho = 2 \times 10^3$ kg/m^3.

B. Numerical protocol

We start our simulations from a set of nonoverlapping particles located at random positions in a periodically repeated cubic box with an initial volume fraction around $\phi \approx 0.2$. The box is compressed isotropically by constant compression rate γ until a given volume fraction, ϕ, is reached. Then the compression is turned off and the system is allowed
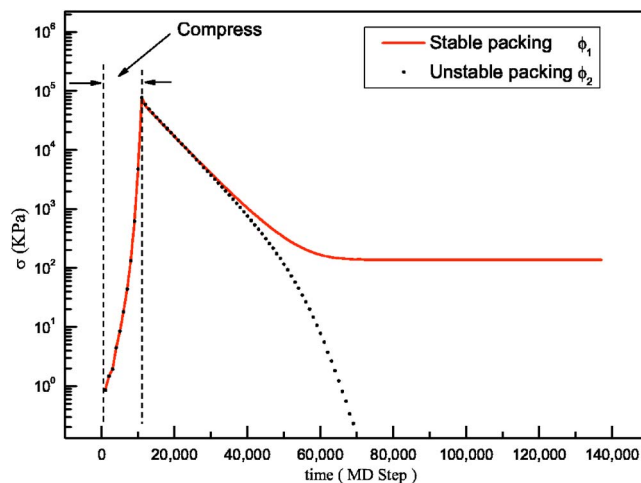

FIG. 3. (Color online) Time evolutions of pressure for two packings in simulation of granular material. Line represents a packing with $\phi_1 > \phi_c$ and circles represent a packing with $\phi_2 < \phi_c$, where $\phi_1 = \phi_2 + 1.6 \times 10^{-5}$.

to relax with constant volume until it reaches a stable state, which means that the pressure of system remains unchanged over a period of time (usually 5×10^5 MD steps). This protocol can generate packings with different volume fractions. From simulations, we find that there is a critical volume fraction ϕ_c, below which a jammed packing with nonzero pressure can not be obtained. This fact is illustrated in Fig. 3, where the time evolution of the pressure in this compress-and-relax process for two packings is shown. The packing with $\phi_1 > \phi_c$ stabilizes at nonzero pressures but the pressure decreases very fast to zero for $\phi_2 < \phi_c$, even though ϕ_1 and ϕ_2 are different only by 1.6×10^{-5}.

Several other ways of preparing static packings of particles exist in the literature. Conjugate gradient methods were used to study dense random packing of frictionless particles by O'Hern et al. [14]. A pouring-ball method, which mimics the process of pouring balls into a container under gravity, was used by Silbert et al. [28,29]. A servo mechanism which adjusts the strain in the system to equilibrate the packing at a given stress was used in [19]. One of the advantages of the present protocol is that it allows us to generate packings with different construction histories by using different compression rates. Thus we can study the path dependency systematically.

C. Computation of characteristic quantities

After generating the packings, we compute the following quantities to characterize their micromechanical and structural properties.

1. Pressure and coordination number

The macroscopic stress tensor for point contacts in a volume V is given by

$$\sigma_{ij} = \frac{1}{V} \sum_k R^k n_i^k F_j^k$$

where V is the volume of the system, $\vec{R}^k$ is the vector joining the center of two particles in contact k, $\vec{n}_k = \vec{R}^k / R^k$, and $\vec{F}^k$ is

the total force in contact k. The pressure σ is the average of three diagonal elements of the stress tensor, i.e., $\sigma = (\sigma_{11} + \sigma_{22} + \sigma_{33})/3$. The coordination number Z is the average of contacts per particle in the contact network, $Z = 2M/N$, where M is the total number of contacts and N is the total number of particles in the contact network. Due to the nongravity environment in our simulation, some floaters, which have zero contacts and do not participate in the contact network, exist. We exclude them when calculating the coordination number. We note the floaters were also reported in Ref. [14].

2. Force distributions, force chains, and participation number

In both emulsion and granular packing, interparticle forces are highly inhomogeneous. This is quantified by the probability distribution of the normal and tangential forces calculated for emulsions and grains. Moreover, photoelastic visualization experiments [30] and simulations [13,31,32] have shown that the contact forces are strongly localized along "force chains" which carry most of the applied stress. To quantify the degree of force localization, we consider the participation number Γ [33]:

$$\Gamma = \left(M \sum_{i=1}^{M} q_i^2 \right)^{-1}. \tag{11}$$

Here M is the number of total contacts, and

$$q_i = f_i / \sum_{j=1}^{M} f_j,$$

where f_j is the total force at contact j. From the definition, $\Gamma = 1$ indicates $q_i = 1/M$, for all q_i and a state with a spatially homogeneous force distribution. On the other hand, in the limit of complete localization, $\Gamma \approx 1/M$, which is essentially zero in our simulation.

3. Plasticity index

In order to quantitatively characterize the tangential forces in the granular packings, we measure the plasticity index following [28]

$$\Sigma = \frac{F_t}{\mu F_n}, \tag{12}$$

which has values between 0 and 1. The maximum means the contact is "plastic" and the tangential force is the Coulomb friction; otherwise the contact is elastic and the tangential force is the Mindlin elastic force.

IV. RESULTS

A. Power-law scaling near jamming, effect of construction history, and isostaticity

In this section, we first show the power-law scaling observed in simulations and the interpretation of the obtained power indices. Then, we discuss the effect of construction history in granular materials. In the third part, we show how our understanding of the effect of construction history can

help to recover isostaticity in granular materials.

Using the protocol discussed above, we generate series of packings of emulsions and granular materials approaching the jamming transition. In order to study the effect of construction history, different compression rates are used to generate the packings. For the case of granular materials, we use four compression rates, $2 \times 10^4, 2 \times 10^3, 2 \times 10^2$, and 2×10 m/s, while for emulsions we use two, 1.5×10^{-2} and 1.5×10^{-3} m/s. Compression rates 2×10 m/s in granular materials and 1.5×10^{-3} m/s in emulsions correspond, respectively, to compressing 1×10^{-7} and 6.7×10^{-8} of a particle diameter per MD step in one spatial direction. Due to the different stiffness of emulsions and granular materials, similar compression rates in units of particle diameters per MD step correspond to quite different values in unit of m/s. In Fig. 4 we plot the pressure σ and coordination number Z of the resulting packings as a function of volume fraction ϕ, where different symbols correspond to different compression rates. Quantitative analysis of the data in Fig. 4 shows that in both cases the pressure σ and extra contacts $Z - Z_c$ vanish as power laws as ϕ approaches the jamming transition at ϕ_c as shown in [13],

$$\sigma \sim (\phi - \phi_c)^\alpha, \tag{13}$$

and

$$Z - Z_c \sim (\phi - \phi_c)^\beta. \tag{14}$$

The power-law fits are shown by lines in Fig. 4 and the extracted fitting parameters including the critical volume fraction ϕ_c, the critical (minimal) coordination number Z_c and two power indices α and β are listed in Table I.

As shown in Fig. 4, the jamming transition for emulsions occurs at $\phi_c = 0.645$ and $Z_c = 6$ regardless of the compression rate, i.e., the construction history. We identify $\phi_c = 0.645$ as the random close packing volume fraction, whose value has been reported many times before [13,14,28]. The minimal coordination number $Z_c = 6$ indicates that the packings near the jamming transition in emulsions are isostatic [13,14,34,28].

A packing is isostatic [35] when the number of contact forces equals the number of force balance equations. In a 3D packing of perfectly smooth (frictionless) particles there are $NZ/2$ unknown normal forces and $3N$ force balance equations. This gives rise to a minimal coordination number needed for mechanical stability as $Z_c = 6$ in 3D (the isostatic limit). In the case of packings of perfectly rough particles, which is realized by frictional particles with infinite friction $\mu \to \infty$ [notice that in this case there are still tangential forces given by the Mindlin elastic component Eq. (2)], in addition to $NZ/2$ unknown normal forces and $3N$ force balance equations, there are NZ unknown tangential forces and $3N$ torque balance equations. Thus the coordination number in the isostatic limit is $Z_c = 4$ for frictional packings in 3D. In such isostatic packings, there is possibly a unique solution for the forces between particles for a given geometrical configuration, because the number of equations equals the number of unknowns. The existence of isostaticity is the foundation of recent theories of stress propagation in granular materials [36–38].
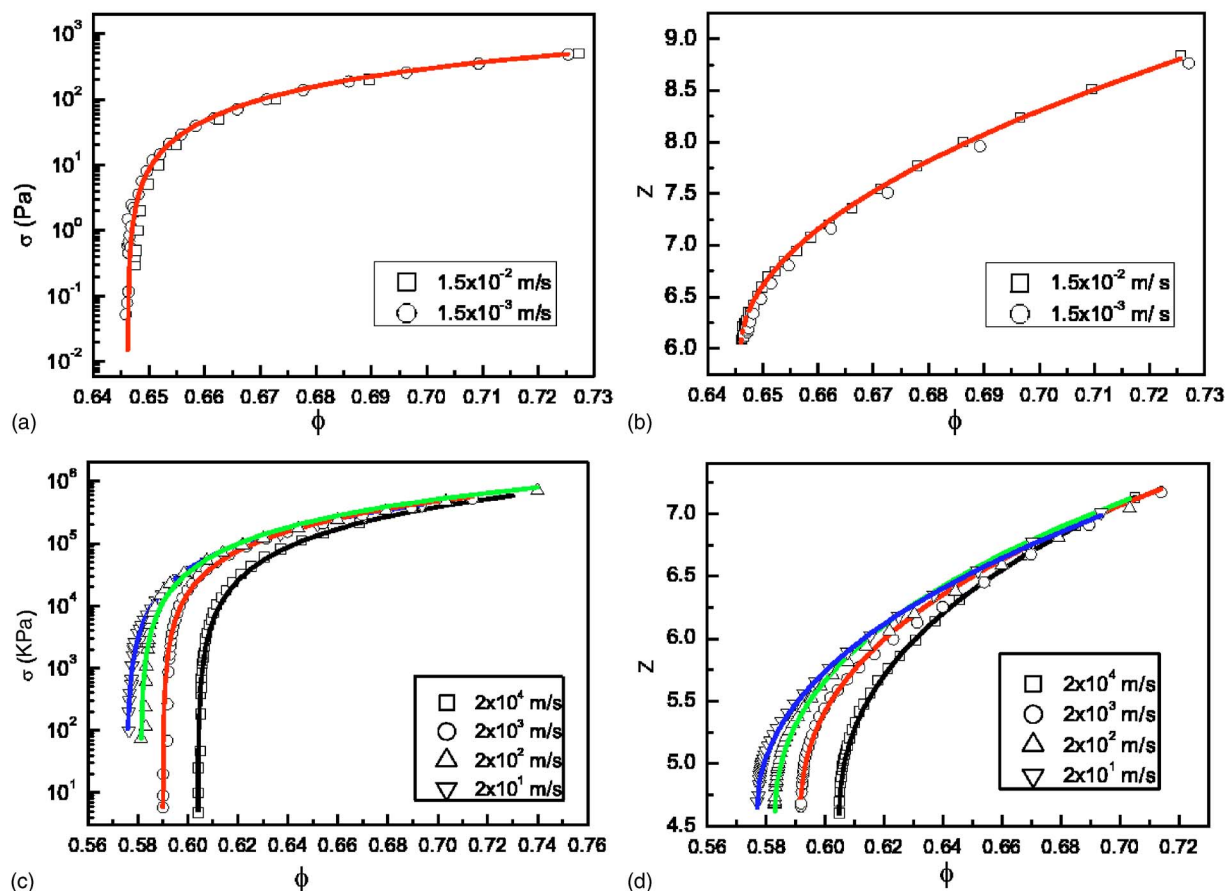
FIG. 4. (Color online) Power-law scalings in the packings of granular materials and emulsions approaching the jamming transition. The symbols are the data from the simulations and different symbol corresponds to different compression rate. The lines are power-law fits. (a) σ vs ϕ in emulsions, (b) Z vs ϕ in emulsions, (c) σ vs ϕ in granular materials, and (d) Z vs ϕ in granular materials.

Thus, in our simulation the isostatic limit in the frictionless case is approached as $\sigma \to 0$ or $\phi \to \phi_c$. In other words, the isostaticity appears in the limit of rigid balls, or when the rigidity of the particles goes to infinity. This corresponds to the so-called marginal rigidity state [38].

Quite different from the results is emulsions, ϕ_c in frictional granular materials with finite $\mu=0.3$ varies depending on the compression rates from 0.576 (slowest rate) to 0.604 (fastest rate) as seen in Fig. 4. The critical coordination numbers in Table I for granular materials are around $Z_c \approx 4.5$.

This value is above $Z_c=4$, the value required by isostaticity. However, it does not mean that these frictional granular packings with finite $\mu=0.3$ are not isostatic since the prediction $Z_c=4$ is strictly valid for packings with $\mu \to \infty$. We will elaborate more on this result below and discuss this limit in more detail.

Next we try to understand the values of the power indexes. In the granular systems, due to the Coulomb cutoff (with $\mu=0.3$), the intergranular normal forces are always larger than the tangential forces. The main contribution to the

TABLE I. Parameters in the power-law fittings near the jamming transition from Eqs. (13) and (14) for emulsions and granular materials.

System	Compression rate (m/s)	ϕ_c	Z_c	α	β
Emulsion, $\mu=0$	$1.5 \times 10^{-2} (10^{-3})$	0.645	6.01	1.25	0.51
Granular, $\mu=0.3$	2×10^4	0.604	4.52	1.52	0.46
Granular, $\mu=0.3$	2×10^3	0.590	4.53	1.46	0.45
Granular, $\mu=0.3$	2×10^2	0.581	4.53	1.48	0.46
Granular, $\mu=0.3$	2×10^1	0.576	4.54	1.52	0.47
Granular, $\mu=\infty$	2×10^2	0.571	3.98	1.66	0.45

pressure is from the normal forces and not the tangential ones. Therefore, for Hertzian balls we expect the following scaling:

$$\sigma \sim F_n \sim \xi^{3/2} \sim (\phi - \phi_c)^{3/2},$$

which implies that the exponent α in Eq. (13) should be equal to the 3/2 exponent of the normal force law in Eq. (1). The values of α obtained in our simulations for different compression rates shown in Table I are all around 3/2, supporting the above argument. This argument should also hold in the case of emulsions since only normal forces act between the droplets. In fact, we get $\alpha = 1.25$ for emulsions independent of the compression rate which is close to the exponent 1.28 in the force law Eq. (8). We note that in frictionless simulations using a linear spring as the force law, $\alpha = 1.05$ is obtained. From Table I we find that the exponents β in Eq. (14) are very close to 0.5 for both emulsions and grains, independent of the force law and also of the compression rate. This numerical value and the independence of the force law were also reported by O'Hern *et al.* [15]. These authors provided a possible way to understand $\beta = 0.5$. In [28] it was shown that the radial distribution function $g(r)$ in packings near the jamming transition displays a power-law behavior near $r = D$, where D is the diameter of the spheres:

$$g(r) \propto (r/D - 1)^{-0.5}. \quad (15)$$

If one assumes an affine deformation upon compression, then one consequence of Eq. (15) is that the coordination number should increase with the power $\beta = 0.5$. However, as shown below, we do not observe the power-law region in $g(r)$ from our data. Therefore, in our opinion, the origin of $\beta = 0.5$ is still not clear. In [19] we provide a more detailed analysis of this argument assuming a narrow peak of the pair distribution function at $r = D$. However, the predicted dependence of the coordination number on pressure still disagrees with the $\beta = 0.5$ result.

Here we elaborate further on the topic and present an analogous derivation of the exponent β. Let us assume that, in the limit of zero pressure, there is a probability distribution $P(h)$ of gap sizes h between each ball and its neighbors:

$$P(h) = Z_c \delta(h) + d_1 h^{-\xi}, \quad (16)$$

which is consistent with a power law in $g(r)$ as given by Eq. (15). In [19] we considered a δ function followed by a Taylor expansion around $h = 0$ instead of the singular behavior of Eq. (16). Following the derivations in [19], which employ an effective-medium approximation that assumes an affine motion of the grains with the external perturbation (being compression of shear), we arrive at the pressure expressed in terms of the static compressive strain $\epsilon < 0$ as

$$\sigma = \frac{\phi k_n}{6\pi} [Z_c(-\epsilon)^{3/2} + d_1(-\epsilon)^{5/2 - \xi}], \quad (17)$$

and the coordination number becomes

$$Z = Z_c + d_3 \sigma^{(2/3)(1-\xi)}. \quad (18)$$

This last result is consistent with Eqs. (13) and (14) with $\beta/\alpha = (2/3)(1-\xi)$. Thus a value of $\xi = 0.5$ would fit all our
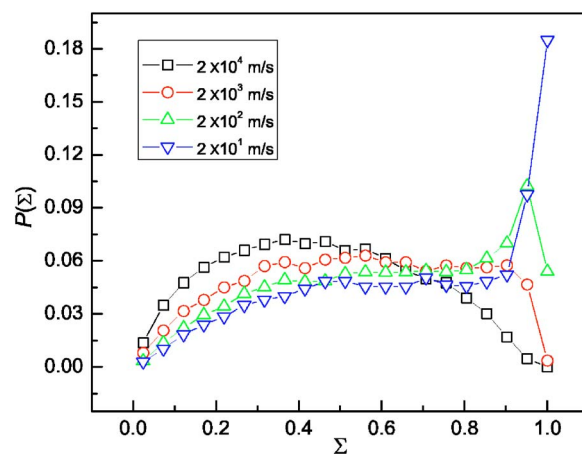

FIG. 5. (Color online) Distributions of Σ parameter. The measurements are carried out on four packings around 650 kPa generated by different compression rates.

data. However, we could not find evidence of Eq. (16) in our simulations.

As we discussed in Sec. II, the tangential forces in the Hertz-Mindlin model are proportional to the normal displacements and therefore depend on the history of interaction. The history dependence shown in Figs. 4(c) and 4(d) for the granular packings is a result of this microscopic path dependence. In our simulations, a lower compression rate allows the grains to have enough time to relax and slide against each other during the preparation protocol. This allows for larger tangential displacement between the grains. On the other hand, a higher compression rate "freezes" the system so quickly that the grains have no time to slide. Thus we expect that the tangential force will be smaller in the packing generated by fast compression rates. In order to quantify this idea, we measured the plasticity index Eq. (12) $\Sigma = F_t / \mu F_n$ for four packings around 650 kPa generated by
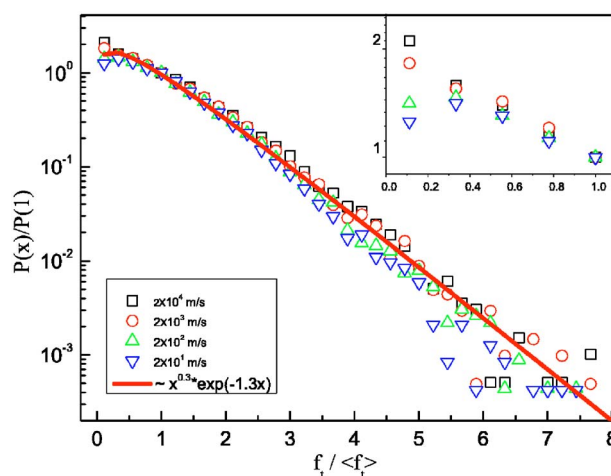

FIG. 6. (Color online) Probability distribution of the tangential forces in packings generated by different compression rates. The X and Y axes are scaled by the averaged force and the probability of the averaged force, respectively. This scaling convention will be used in all the probability distribution plots of forces throughout the paper.
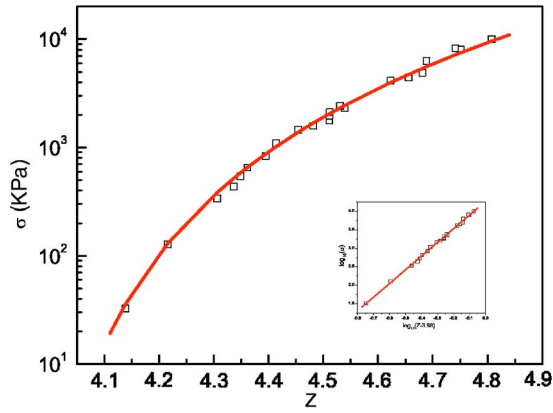
FIG. 7. (Color online) σ vs Z in the packings of granular material in the infinite friction limit.

different compression rates. The probability distributions $P(\Sigma)$, shown in Fig. 5, confirm the above argument. In the packing generated by $\gamma = 2 \times 10$ m/s, almost 20% of the tangential forces are truncated by the Coulomb cutoff as evidenced by the fact that $P(\Sigma)$ has a maximum at $\Sigma = 1$. On the other hand, for the fastest compression rate $\gamma = 2 \times 10^4$ m/s, the peak of the distribution is around $\Sigma \approx 0.4$ and $P(\Sigma = 1)$

≈ 0, implying that there are almost no plastic contacts. This indicates that the grains in the packing generated by lower compression rates feel more "sticky" to each other; therefore the packings can sustain nonzero pressure at lower volume fraction. This explains why ϕ_c decreases as γ decreases in granular materials. In Fig. 6, we plot the probability distribution functions of the tangential forces in the packings generated by different compression rates. The distributions are different in the small force regions. The packing generated by $\gamma = 2 \times 10^4$ m/s contains more small forces, which are less than the average forces, than the packing generated by $\gamma = 2 \times 10$ m/s. This observation can be explained by the argument given above. A lower compression rate produces better developed tangential forces and thus reduces the number of small tangential forces.

We have shown that the critical contact number $Z_c \sim 4.5$ in the packings of granular materials with $\mu = 0.3$ is larger than the prediction of isostatic considerations $Z_c = 4$. We first noticed that $Z_c = 4$ is strictly valid when $\mu \to \infty$. Moreover, we showed above that a fast compression rate inhibits the developments of tangential forces and therefore may also contribute to the breakdown of isostaticity. Therefore, we now investigate the slow compression rate limit of a granular packing in the $\mu \to \infty$ limit. We carried out a set of simula-
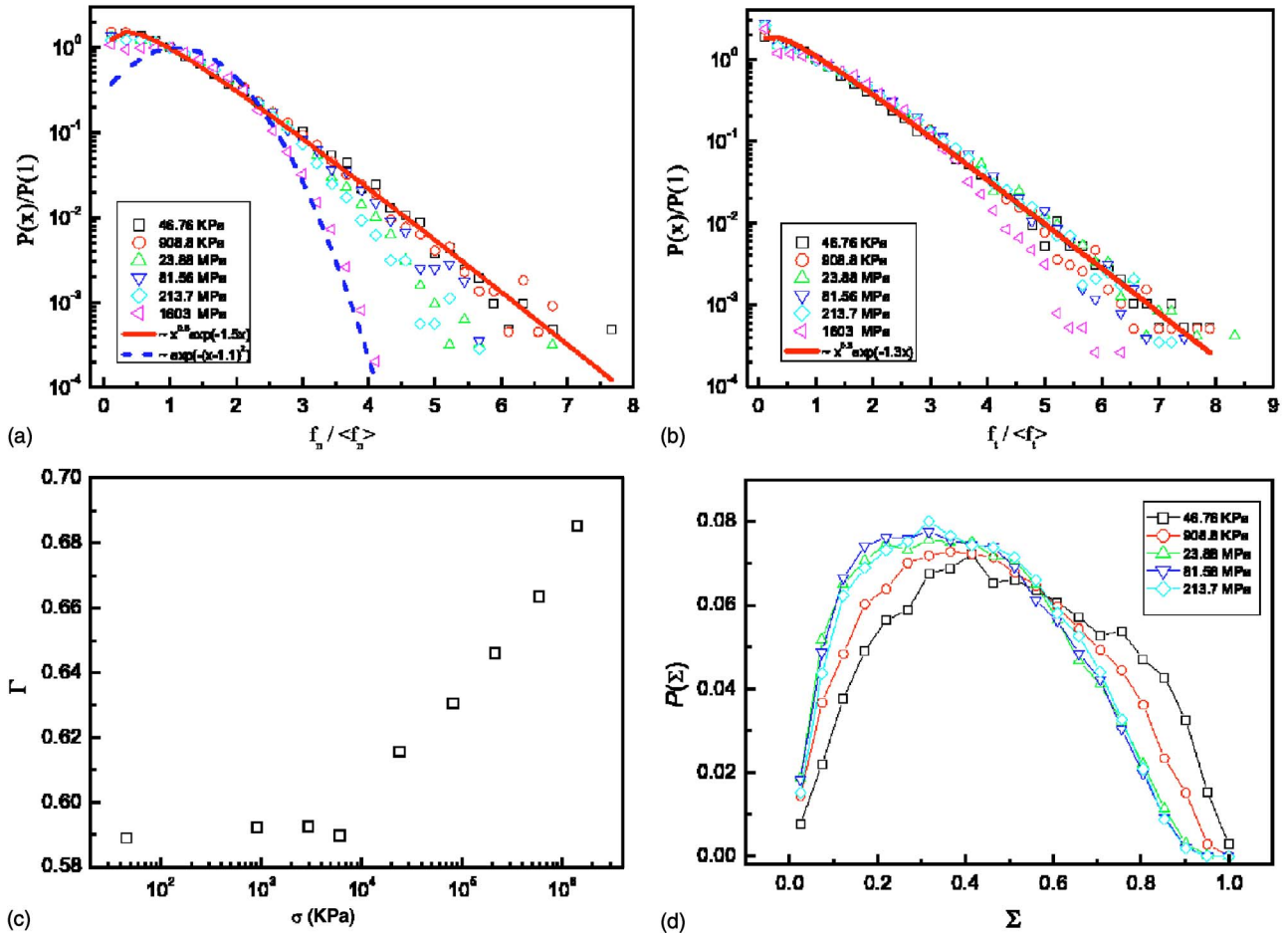

FIG. 8. (Color online) Micromechanical properties at different pressures in the packings of granular materials. Measurements are carried on the packings generated by $\gamma = 2 \times 10^4$ m/s. (a) Distribution of the normal forces; (b) distribution of the tangential forces; (c) Γ (participation number) vs pressure; and (d) distribution of Σ (plasticity index).

tions of grains interacting via Hertz forces Eq. (1) and tangential Mindlin forces Eq. (2) but without the Coulomb cutoff ($\mu = \infty$) for a compression rate $\gamma = 2 \times 10^2$ m/s, slow enough to allow sufficient time for grains to rearrange. The result of the simulations is shown in Fig. 7. The pressure versus volume fraction can be fitted by

$$\sigma \sim (Z - 3.98)^{3.69}, \qquad (19)$$

with a minimal coordination number $Z_c = 3.98$ indicating the recovery of isostaticity. We find $\phi_c = 0.571$ and exponents $\alpha = 1.66$ and $\beta = 0.45$. We also find that Z_c is larger than 4 if a compression rate larger than $\gamma = 2 \times 10^2$ m/s is used. This may also suggest that the lack of isostaticity found in [29] for frictional packings might be due to the fast preparation protocol inherent to the pouring-ball method.

Finally, we note that, in addition to Σ and the probability distribution function of tangential forces, we also measure the normal force distribution, coordination number distribution and radial distribution function for the four packings around 650 kPa at different compression rates and found no clear signature of history dependency in these measurements.

B. Micromechanical and microstructural properties

In order to study the micromechanical and microstructural properties near the jamming transition we carry out the measurements described in Sec. II B. For the micromechanical properties, we measure the normal and tangential force distributions [20,29,30,32] and the Γ [13] and Σ parameters [28]. For the microstructural properties we calculate the distribution of contacts and the radial distribution function. In this subsection, we will show the results of the above measurements carried on the packings generated by $\gamma = 1.5 \times 10^{-3}$ m/s for emulsions and $\gamma = 2 \times 10^4$ m/s for granular materials. The measurements done on the packings generated by other γ's are basically the same.

1. Micromechanical properties

The normal force distributions in emulsions and granular materials at different pressures are plotted in Figs. 8 and 9, respectively, as a function of the magnitude of forces normalized by the average forces. At low pressures, the distributions show a plateau below the average force which has been considered as the signature of the jamming transition [14]. The distributions show a broad exponential tail for forces larger than the average which extend up to eight times the average force for the packings with the lowest pressures. On the other hand, the Γ parameters in Figs. 8(c) and 10 have small values at low pressures, which means the forces are distributed heterogeneously in space, i.e., they are localized. Combining the information from the force distributions and the Γ parameter we may conclude that at low pressures there are very large forces in the packings and the forces are distributed heterogeneously. This agrees with the picture of force chains, which have been visualized in granular matter in both experiment [30] and simulations [13,31,32]. As shown in [13], these force chains sustain most of the external loading. At low pressures, the number of the force chains are small and they are well separated [13]. We also point out that the ex-
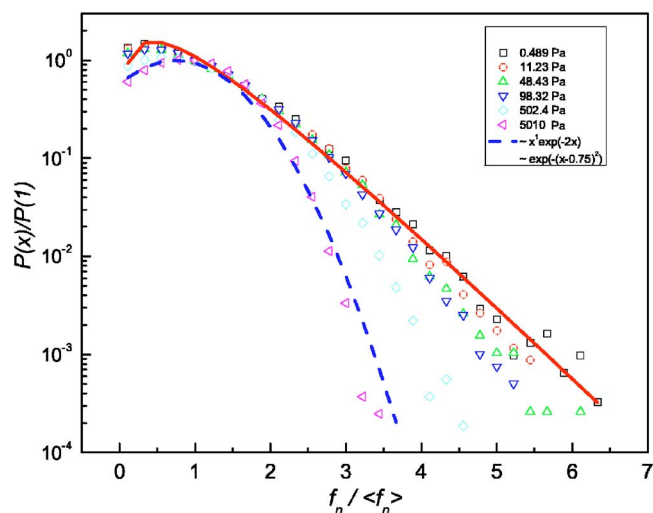

FIG. 9. (Color online) Distribution of the normal forces in emulsions. Measurements were carried on the packings generated by $\gamma = 1.5 \times 10^{-3}$ m/s.

periments with confocal microscopy of compressed emulsions systems [20] did not find evidence of force chains in the bulk. Our computer simulations of frictionless grains could not reproduce these results as we find evidence of localization even for frictionless droplets.

As the pressure increases, the force distributions get narrow; the exponential tails bend down and transform into a Gaussian-like one, as shown by the fitting of the dashed lines in Figs. 8(a) and 9 for grains and emulsions. The deviation from the exponential tail indicates that the very large forces (in comparison with the average force) are disappearing. At the same time, Γ increases sharply with pressure in Figs. 8(c) and 10, which indicates that the packing is becoming homogeneous. This sharp increase happens roughly at 10 MPa for granular materials and 50 Pa for emulsions. Similar behavior of Γ has also been reported in [13] for grains and the increase of Γ was understood as the indication of the disappearance of well-separated force chains.
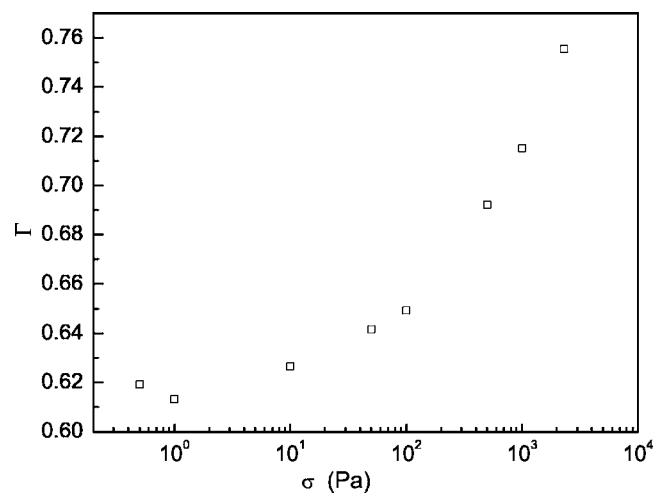

FIG. 10. Γ vs pressure in emulsions. Measurements were carried on the packings generated by $\gamma = 1.5 \times 10^{-3}$ m/s.
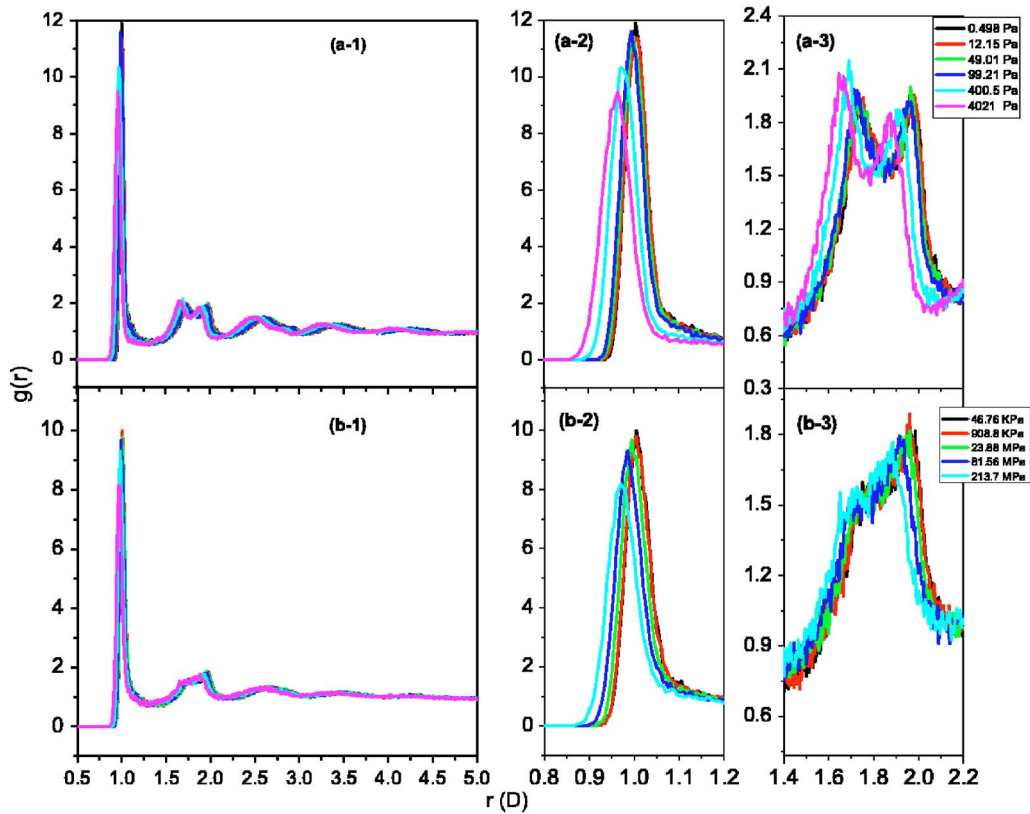
FIG. 11. (Color online) Radial distribution functions in the packings of emulsions and granular materials; *X* axis is in units of particle diameter. (a-1) The complete RDF in granular matter; (a-2), (a-3) the first and second peaks of the RDF in granular materials; (b-1) the complete RDF in emulsions; (b-2), (b-3) the first and second peaks of the RDF in emulsions.

The distribution at low pressures, containing a plateau and the exponential tail, can be fitted by various expressions. Here we choose one from [20],

$$P(f) = af^\lambda \exp[-(1+\lambda)f].$$

This expression comes from a simple Boltzmann equation theory and the power-law coefficient λ is determined by the packing geometry of the system. The fits are shown as solid lines in the plots.

The tangential force distributions in granular materials also show exponential tails and their pressure dependence is weaker than in the normal force distributions, as seen in Fig. 8(b). The distributions of Σ are plotted in Fig. 8(d) for five pressures. As the pressure decreases, the distribution of Σ
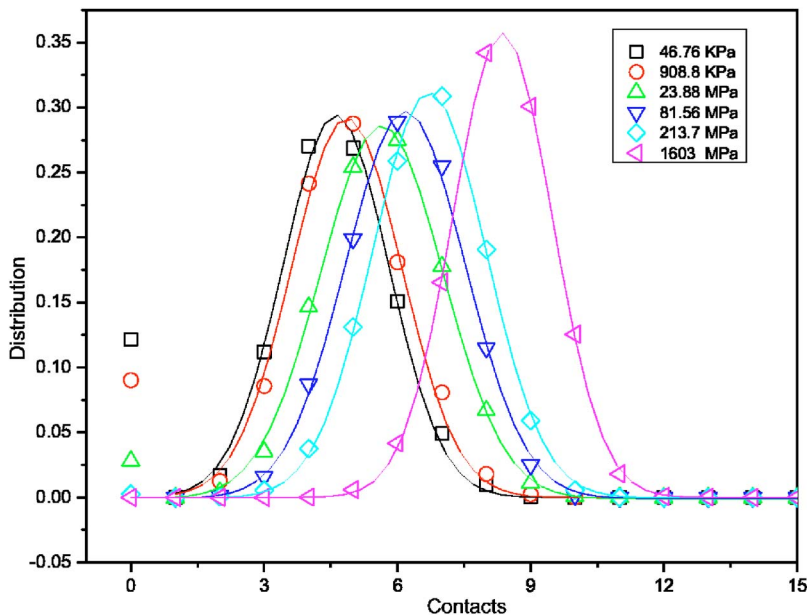

FIG. 12. (Color online) Distribution of contacts in the packings of granular materials. The lines are Guassian fits to the distributions, with the floaters excluded.
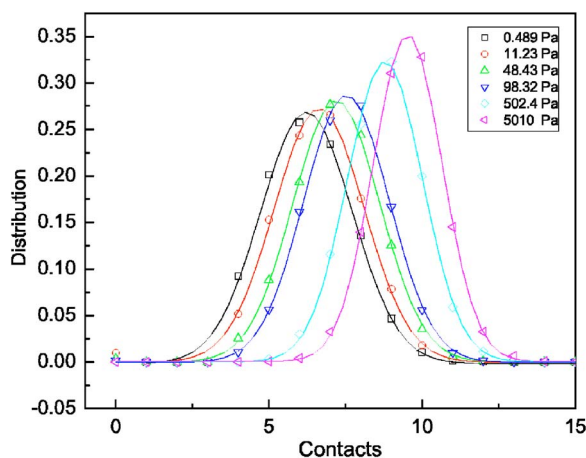
FIG. 13. (Color online) Distribution of contacts in the packings of emulsions. The lines are Guassian fits to the distributions, with the floaters excluded.

shifts slightly to higher values. This is due to the fact that, in our protocol, the system arrests itself more quickly during the construction of high-pressure packings than in low-pressure cases. Therefore, the particles in packings at lower pressures have more time to slide and have larger tangential displacements; therefore larger tangential forces.

2. Microstructural properties

The radial distribution function (RDF) describes how the particles are distributed radially. In Fig. 11, the radial distribution functions show prominent peaks at $r=r_0$, a second peak at $r=2r_0$, and a subpeak approximately at $r=\sqrt{3}r_0$. As the system approaches the jamming transition from high pressures, the distribution functions shift to the right due to the increase of system size [Figs. 11(a-1) and 11(b-1) for emulsions and grains, respectively). The first peak decreases in width and increases in height, as shown in Figs. 11(a-2) and 11(b-2). However, we do not find a tendency for the first peak to evolve into a δ function as reported in [15]. In [28] Silbert *et al.* reported the power-law behavior of Eq. (15) near the first peak in granular materials. However, from our data we cannot clearly identify this power-law region. At low pressures we find $r_o \approx D$, which means that the particles barely touch each other.

The splitting of the second peak in the RDF observed in Figs. 11(a-3) and 11(b-3) has been reported by various authors studying dense liquids and granular materials [26,39–42]. The authors of Ref. [39] considered this splitting to be a structural precursor to the freezing transition and the development of long-range order. They attributed this splitting to four-particle hexagonally close-packed arrangements, which help the system to lower its energy. From Figs. 11(a-3)

and 11(b-3), we see that the subpeaks in granular materials are less pronounced than in emulsions. This indicates that the tangential forces prevent the formation of these four-particle clusters.

The distributions of contacts are shown in Fig. 12 for granular materials and in Fig. 13 for emulsions. Both distributions can be fitted by Gaussians. As the pressure is increased the distributions move to the right and get slightly narrower. Floaters (those particles with zero coordination number) exist in granular materials at low pressure (around 12% at 46.74 kPa) while the fraction of floaters is much lower (2% at 0.498 Pa) in emulsions. As expected the number of floaters decreases as pressure increases. Excluding the floaters, we can fit the distributions with a Gaussian function, as shown by the lines in Figs. 12 and 13. We note that similar results on the distribution of contacts have been reported in [43].

V. SUMMARY

We have studied the jamming transition in packings of emulsions and granular materials via molecular dynamics simulations. Power-law scaling is found for the vanishing of the pressure and excess number of contacts as the system approaches the jamming transition from high volume fractions. The emulsion system jams at $\phi_c=0.645$ independent of the construction histories while granular materials jam at ϕ_c between 0.576 and 0.604 depending on the construction histories. We found that the preparation protocol has a strong effect on the tangential forces in granular materials. Longer construction times of the packings allow the particles to relax and slide against each other and therefore to have larger tangential displacements, which lead to larger tangential forces. Isostaticity is found in the packings close to the jamming transition in emulsions and in granular materials in the limit of infinite friction and slow compression rate. Heterogeneity of the force distribution increases while the system approaches the jamming transition, demonstrated by the exponential tail in the force distributions and the small values of the participation number. However, no signatures of jamming transitions are observed in structural properties, like the radial distribution functions and the distributions of contacts.

[1] *Jamming and Rheology: Constrained Dynamics on Microscopic Scales*, edited by A. J. Liu and S. R. Nagel (Taylor & Francis, London, 2001).

[2] H. A. Makse, J. Brujić, and S. F. Edwards, in *The Physics of Granular Media*, edited by H. Hinrichsen and D. E. Wolf (Wiley-VCH, Weinheim, 2004).

[3] *Unifying Concepts in Granular Media and Glasses* edited by A. Coniglio, A. Fierro, H. J. Herrmann, and M. Nicodemi (Elsevier, Amsterdam, 2004).

[4] J. D. Bernal, Nature (London) **188**, 910 (1960)

[5] G. D. Scott, Nature (London) **188**, 908 (1960);J. L. Finney, Proc. R. Soc. London, Ser. A **319**, 479 (1970);J. G. Berryman, Phys. Rev. A **27**, 1053 (1983).

[6] G. Y. Onoda and E. G. Liniger, Phys. Rev. Lett. **64**, 2727 (1990).

[7] M. D. Rintoul and S. Torquato, Phys. Rev. Lett. **77**, 4198 (1996).

[8] S. F. Edwards, in *Granular Matter: An Interdisciplinary Approach*, edited by A. Mehta (Springer, New York, 1994), pp. 121–140.

[9] A. Mehta and S. F. Edwards, Physica A **157**, 1091 (1989).

[10] J. Kurchan, J. Phys.: Condens. Matter **29**, 6611 (2000).

[11] A. Barrat, J. Kurchan, V. Loreto, and M. Sellitto, Phys. Rev. Lett. **85**, 5034 (2000).

[12] H. A. Make and J. Kurchan, Nature (London) **415**, 614 (2002).

[13] H. A. Makse, D. L. Johnson, and L. M. Schwartz, Phys. Rev. Lett. **84**, 4160 (2000).

[14] C. S. O'Hern, S. A. Langer, A. J. Liu, and S. R. Nagel, Phys. Rev. Lett. **88**, 075507 (2001).

[15] C. S. O'Hern, L. E. Silbert, A. J. Liu, and S. R. Nagel, Phys. Rev. E **68**, 011306 (2003).

[16] V. Trappe, V. Prasad, L. Cipelletti, P. N. Segre, and D. A. Weitz, Science **411**, 772 (2001).

[17] L. D. Landau and E. M. Lifshitz, *Theory of Elasticity* (Pergamon, New York, 1970).

[18] R. D. Mindlin, J. Appl. Math. **71**, 259 (1949).

[19] H. A. Makse, N. Gland, D. L. Johnson, and L. M. Schwartz, Phys. Rev. E **70**, 061302 (2004).

[20] J. Brujić, S. F. Edwards, I. Hopkinson, and H. A. Makse, Physica A **327**, 201 (2003);J. Brujić, S. F. Edwards, D. V. Grinev, I. Hopkinson, D. Brujić, and H. A. Makse, Faraday Discuss. **123**, 207 (2003).

[21] E. R. Nowak, J. B. Knight, E. Ben-Naim, H. M. Jaeger, and S. R. Nagel, Phys. Rev. E **57**, 1971 (1998).

[22] K. L. Johnson, *Contact Mechanics* (Cambridge University Press, Cambridge, U.K., 1985).

[23] H. M. Princen, J. Colloid Interface Sci. **91**, 160 (1983).

[24] D. C. Morse and T. A. Witten, Europhys. Lett. **22**, 549 (1993).

[25] M-D. Lacasse, G. S. Grest, D. Levine, T. G. Mason, and D. A. Weitz, Phys. Rev. Lett. **76**, 3448 (1996).

[26] T. G. Mason, J. Bibette, and D. A. Weitz, Phys. Rev. Lett. **75**, 2051 (1995).

[27] P. A. Cundall and O. D. L. Strack, Geotechnique **29**, 47 (1979).

[28] L. E. Silbert, D. Ertas, G. S. Grest, T. C. Halsey, and D. Levine, Phys. Rev. E **65**, 051307 (2002).

[29] L. E. Silbert, D. Ertas, G. S. Grest, T. C. Halsey, and D. Levine, Phys. Rev. E **65**, 031304 (2002).

[30] C. H. Liu, S. R. Nagel, D. A. Schechter, S. N. Coppersmith, S. Majumdar, O. Narayan, and T. A. Witten, Science **269**, 513 (1995).

[31] F. Radjai, M. Jean, J. Moreau, and S. Roux, Phys. Rev. Lett. **77**, 274 (1996).

[32] S. J. Antony, Phys. Rev. E **63**, 011302 (2000).

[33] J. S. Andrade, Jr., U. M. S. Costa, M. P. Almeida, H. A. Makse, and H. E. Stanley, Phys. Rev. Lett. **82**, 5249 (1999).

[34] C. F. Moukarzel, Phys. Rev. Lett. **81**, 1634 (2000).

[35] S. Alexander, Phys. Rep. **296**, 65 (1998).

[36] S. F. Edwards and D. V. Grinev, Phys. Rev. Lett. **82**, 5397 (1999).

[37] A. Tkachenko and T. A. Witten, Phys. Rev. E **60**, 687 (1999).

[38] R. C. Ball and R. Blumenfeld, Phys. Rev. Lett. **88**, 115505 (2002).

[39] T. M. Truskett, S. Torquato, S. Sastry, P. G. Debenedetti, and F. H. Stillinger, Phys. Rev. E **58**, 3083 (1998).

[40] A. S. Clarke and H. Jónsson, Phys. Rev. E **47**, 3975 (1993).

[41] W. Kob and H. C. Anderson, Phys. Rev. E **51**, 4626 (1995).

[42] H. Li, X. Bian and G. Wang, Phys. Rev. B **67**, 094202 (2003).

[43] T. G. Mason, Martin-D. Lacasse, Gary S. Grest, Dov Levine, J. Bibette, and D. A. Weitz, Phys. Rev. E **56**, 3150 (1997).